Cellular/Molecular

# Lysosomes Are the Major Vesicular Compartment Undergoing $Ca^{2+}$-Regulated Exocytosis from Cortical Astrocytes

**Dongdong Li,**[1,2,3] **Nicole Ropert,**[1,2,3] **Annette Koulakoff,**[4,5] **Christian Giaume,**[4,5] **and Martin Oheim**[1,2,3]

[1]Institut National de la Santé et de la Recherche Médicale (INSERM), Unité 603, and [2]Centre National de la Recherche Scientifique, Unité Mixte de Recherche 8154, and [3]Université Paris Descartes, Laboratory of Neurophysiology and New Microscopies, F-75006 Paris, France, and [4]INSERM, Unité 840, and [5]Collège de France, F-75005 Paris, France

**Although $Ca^{2+}$-dependent exocytosis is considered to be a pathway for gliotransmitter release from astrocytes, the structural and functional bases of this process remain controversial. We studied the relationship between near-membrane $Ca^{2+}$ elevations and the dynamics of single astroglial vesicles with styryl (FM) dyes. We show that cultured astrocytes, unlike neurons, spontaneously internalize FM dyes, resulting in the labeling of the entire acidic vesicle population within minutes. Interestingly, metabotropic glutamate receptor activation did not affect the FM labeling. Most FM-stained vesicles expressed sialin, CD63/LAMP3, and VAMP7, three markers for lysosomes and late endosomes. A subset of lysosomes underwent asynchronous exocytosis that required both $Ca^{2+}$ mobilization from intracellular stores and $Ca^{2+}$ influx across the plasma membrane. Lysosomal fusion occurred within seconds and was complete with no evidence for kiss and run. Our experiments suggest that astroglial $Ca^{2+}$-regulated exocytosis is carried by lysosomes and operates on a timescale orders of magnitude slower than synaptic transmission.**

*Key words:* **glia; vesicle release; intracellular signaling; total internal reflection fluorescence microscopy; TIRF; kiss and run; readily releasable pool**

## Introduction

Fast $Ca^{2+}$-regulated exocytosis has been regarded as a specialized process for transmitter release from neurons and neuroendocrine cells. However, recently, there has been a surge in research concerning exocytosis from astrocytes. In addition to their established functions (Bergles et al., 1999; Simard and Nedergaard, 2004; Gordon et al., 2007; Hertz et al., 2007), these glial cells release various transmitters that exert a feedback control on neuronal activity (Fellin and Carmignoto, 2004; Volterra and Meldolesi, 2005) (but see Fiacco et al., 2007). Astrocytes have been shown to release glutamate after $Ca^{2+}$ uncaging (Kreft et al., 2004; Perea and Araque, 2007), mechanical (Chen et al., 2005) or electrical stimulation (Jourdain et al., 2007), and in response to the application of prostaglandin (Bezzi et al., 1998), DHPG (dihydroxyphenylglycine) (Bezzi et al., 2004), ATP (Zhang et al., 2004a,b), or glutamate (Chen et al., 2005). This $Ca^{2+}$-regulated pathway shares features with neuronal exocytosis (for review, see Volterra and Meldolesi, 2005; Haydon and Carmignoto, 2006; Montana et al., 2006). In addition to releasing glutamate, astrocytes can respond to increases of the intracellular free calcium concentration ($[Ca^{2+}]_i$) with the vesicular release of ATP (Coco et al., 2003; Pangrsic et al., 2007; Zhang et al., 2007; Pryazhnikov and Khiroug, 2008), D-serine (Mothet et al., 2005), and neuroactive peptides (Krzan et al., 2003). The ultrastructural and functional bases for astroglial secretion remain uncertain and little is known about the dynamics, trafficking, and the contents of the different vesicular compartments.

Unlike synaptic terminals, which have dense vesicle clusters, electron micrographs of astroglial processes do not display obvious vesicle accumulations (Nedergaard et al., 2002). Scattered vesicles bearing the type 1 and 2 vesicular glutamate transporters (VGlut1 and VGlut2) were observed near presynaptic nerve terminals (Bezzi et al., 2004; Jourdain et al., 2007). However, because massive exocytosis of these vesicles would have to occur to account for the amount of glutamate released (Bezzi et al., 1998), the functional importance of $Ca^{2+}$-regulated exocytosis from astrocytes has been debated (Takano et al., 2005).

Live-cell studies using evanescent-field or confocal fluorescence microscopy have begun to provide images of single-vesicle dynamics in cultured astrocytes (Bezzi et al., 2004; Bowser and Khakh, 2007; Stenovec et al., 2007; Striedinger et al., 2007; Zhang et al., 2007; Pryazhnikov and Khiroug, 2008), but no coherent view has emerged at this stage. Previous studies identified gluta-

Received Feb. 18, 2008; revised May 14, 2008; accepted June 12, 2008.

This work was supported by the Groupement d'Intérêt Publique–Agence Nationale de la Recherche (GIP-ANR) Neurosciences "ASTREX", a joint Franco-German Institut de la Santé et de la Recherche Médicale/Max Planck Society "AMIGO" Grant, and the Bettencourt-Schueller Foundation. D.L. was the recipient of Ministère de la Recherche et de la Technologie and GIP-ANR postdoctoral fellowships. We acknowledge the help of Camilla Luccardini (Paris, France) and Stephanie Rudolph (Göttingen, Germany) with molecular biology. We thank Etienne Audinat, Serge Charpak, Bruno Gasnier, Frank Kirchhoff, Alain Marty, and Corinne Sagné for critical discussion, and JacSue Kehoe for careful corrections.

Correspondence should be addressed to Martin Oheim, Université Paris Descartes, Laboratory of Neurophysiology and New Microscopies, 45 rue des Saints Pères, F-75006 Paris, France. E-mail: martin.oheim@univ-paris5.fr.

DOI:10.1523/JNEUROSCI.0744-08.2008

 0270-6474/08/287648-11$15.00/0

matergic (Bezzi et al., 2004) and VAMP2-expressing small vesicles (Crippa et al., 2006) as well as larger granules of 300–500 nm diameter (Chen et al., 2005; Zhang et al., 2007), suggesting that several vesicular pathways might coexist and contribute to gliotransmitter release. Moreover, recent work has documented in astrocytes the exocytic release of ATP from lysosomal compartments (Jaiswal et al., 2007; Zhang et al., 2007).

Confronted with this diversity of secretory organelles and partially conflicting results, we reexamined in cultured mouse cortical astrocytes the spatial and temporal relationship between the near-membrane intracellular calcium concentration ($[Ca^{2+}]_i$) and the dynamics of vesicular compartments.

Contrary to what was expected by analogy with neuronal vesicle dynamics, cultured astrocytes took up styryl (FM) dyes in the absence of stimulation, and the uptake was not further augmented by the activation of metabotropic glutamate receptors (mGluRs). Within minutes after dye exposure, we observed a complete overlap between FM4-64-labeled and acidic vesicle markers. The vast majority of these organelles expressed lysosomal protein markers and, to a lesser extent, early endosome or secretory vesicle markers. A subpopulation of sialin-enhanced green fluorescent protein (EGFP)/FM4-64 double-labeled organelles fully collapsed into the plasma membrane on submicromolar elevation of $[Ca^{2+}]_i$. Astroglial exocytosis was asynchronous and required the activation of $Gd^{3+}$-sensitive $Ca^{2+}$-permeable channels as well as $Ca^{2+}$ mobilization from the endoplasmic reticulum (ER). Our findings impose important temporal constraints for astroglial vesicular signaling at the tripartite synapse.

## Materials and Methods

*Cell preparation and solutions.* Astrocytes were prepared from postnatal day 0 (P0) to P1 mouse cortex (see supplemental material, available at www.jneurosci.org). Briefly, cerebral cortices were dissected and mechanically dissociated, and cells were plated and cultured for 1 week to reach confluence before their transfer to coverslips. Astrocytes in small islands of one to three cells were recorded from day 2 to 6 after transfer into secondary culture. Most recordings were made at room temperature unless otherwise indicated. During recording, cells were constantly perfused at 0.5–1 ml/min with physiological saline containing the following (in mM): 140 NaCl, 5.5 KCl, 1.8 $CaCl_2$, 1 $MgCl_2$, 20 glucose, 10 HEPES. pH was adjusted to 7.3 (NaOH). Perfusion was stopped during incubations. $Ca^{2+}$-free extracellular solutions contained nominally zero $[Ca^{2+}]_o$ and 2 mM EGTA.

*Fluorescent markers.* We labeled astrocytes with the acidophilic fluorescent weak bases quinacrine (Fluka), Lysotracker Green DND-26 (Invitrogen), acridine orange (AO) (Sigma-Aldrich), and FM2-10, FM1-43, or FM4-64 (Invitrogen). FM staining of external plasma membranes was washed off by thoroughly rinsing the cells during 20 min before viewing. Where indicated, we quenched FM1-43 fluorescence by adding 2 mM bromophenol blue (BPB) (3′,3″,5′,5″-tetrabromophenolsulfophthalein sodium salt; Sigma-Aldrich), an acid–base indicator with $pK_a$ 4.0 and a yellow-to-blue transition between pH 3.0 and 4.6 (supplemental Fig. 3, available at www.jneurosci.org as supplemental material). ER Tracker Blue-White DPX (2 μM; 1 h; Invitrogen) was used to label the endoplasmic reticulum.

*Fluorescent protein expression.* We transfected cultured astrocytes with 1.4 μg/ml cDNA coding for organelle-specific fusion proteins, using Lipofectamine 2000 (Invitrogen), which typically resulted in one-third of the astrocytes expressing fluorescent protein markers. Their expression was under the control of the ubiquitously active cytomegalovirus promoter. We used as organelle markers the following fusion proteins: vesicular-associated membrane proteins VAMP2 (a gift from J. P. Mothet, Institu Fédératif de Neurobiologie Alfred Fessard, Centre National de la Recherche Scientifique, Université Paris Descartes 9040, Bordeaux, France), VAMP3 (from T. Galli, Institut Jacques Monod, Unité Mixte de Recherche 7592, Paris, France) fused on their C terminus to pEGFP-N1 (Clontech), EGFP-sialin (from B. Gasnier, Institut de Biologie Physico-Chimique, Centre National de la Recherche Scientifique, Unité Propre de Recherche 1929, Paris, France), CD63-EGFP, Ti-VAMP/VAMP7-EGFP, endobrevin/VAMP8-EGFP (all from T. Galli). The exposure to low pH of EGFP in the vesicle lumen affects its intensity but not the spectrum (Nadrigny et al., 2006). VGlut1-Venus and VGlut3-Venus (from E. Herzog, Max Planck Institute for Experimental Medicine, Göttingen, Germany) were transfected as markers of glutamatergic vesicles.

Expression was checked the day after transfection by systematically comparing the fluorescence excitation and the five-point emission spectrum of transfected astrocytes with their nonlabeled counterparts from the same preparation (data not shown) (Nadrigny et al., 2006). Controls of the correct targeting of the transfected plasmids were performed with cytoplasmically targeted EGFP (pEGFP-N1; Clontech) (Nadrigny et al., 2006). Neither the number nor the fusion competence of FM-labeled organelles was altered by cell transfection (supplemental Fig. 6, available at www.jneurosci.org as supplemental material).

*Calcium imaging.* $[Ca^{2+}]_i$ was monitored with total internal reflection fluorescence microscopy (TIRF) or epifluorescence using the nonratiometric $Ca^{2+}$ indicator Oregon-Green-BAPTA-1 (OGB-1) ($K_d \sim 170$ nM) after AM-ester loading (2 μM; 30 min), followed by 30 min wash for deesterification. In some experiments, we used the lower-affinity $Ca^{2+}$ indicators Fluo-4 AM (data not shown) ($K_d \sim 325$ nM) or X-rhod-1 AM ($K_{D,Ca} \sim 700$ nM) to confirm that the triggered $[Ca^{2+}]_i$ elevations did not saturate OGB-1. $[Ca^{2+}]_i$ is given as $dF/F_0$, where $F_0$ is the average prestimulus fluorescence after subtraction of the average cellular autofluorescence measured before AM loading. Traces are corrected for photobleaching unless otherwise indicated. Wavelength filter combinations are listed in supplemental Table 1 (available at www.jneurosci.org as supplemental material).

*Quantitative multicolor imaging and colocalization analysis.* We used a custom inverted microscope equipped for brightfield as well as polychromatic epifluorescence and through-the-objective (60×; numerical aperture, 1.45) evanescent-field fluorescence excitation (Nadrigny et al., 2006, 2007). A Polychrome II light source (TILL Photonics) provided monochromatic (18 nm full-width at half-maximum) epifluorescence illumination. For evanescent-field excitation, we used an $Ar^+/Kr^+$ multiline laser (Melles Griot) and an acousto-optical tunable filter for wavelength selection (AOTF; AA Opto Electronic). Laser power was adjusted in function of the exposure time with neutral density filters to avoid photodamage. Typical intensities ranged between <20 μW (for imaging AO-loaded organelles) and 600 μW for 10 Hz imaging of FM4-64. The total illuminated near-membrane section ($1/e^2$-intensity decay) sampled by the evanescent field was on the order of 200 nm. For emission spectral imaging (Nadrigny et al., 2006), five emission spectral images were acquired sequentially on 458 nm excitation (supplemental Fig. 5, available at www.jneurosci.org as supplemental material). Fluorescence images were magnified (2×) and projected onto a highQE GenIII-intensified PentaMax charge-coupled device camera (Roper Scientific). The effective pixel size in the specimen plane was 187 nm. Exposure times were 100–300 ms, and 0.5–1 s for BPB. Most epifluorescence movies were taken at 1 Hz, whereas TIRF images were streamed at 10 Hz. To control for photobleaching, time-lapse images were acquired for each fluorophore loaded in cells under the same conditions used for imaging. The photobleaching rate was derived from the single-exponential fit to control images, and then used to correct fluorescence traces. We systematically quantified the amount of cross talk in multicolor images. Correlation between the staining by FM4-64 and various yellow/green fluorescent markers was assessed by calculating a modified Pearson's coefficient, $\tilde{r}_{12}$, which accounts for image noise, based on the comparison of replicate images. Meaningful upper and lower bounds were established from controls (for details, see supplemental material, available at www.jneurosci.org). All single-vesicle fluorescence intensity was corrected for local background unless otherwise stated.

*Statistics.* Data are expressed as mean ± SD, and the *t* test was used for testing significance of *p* values unless otherwise indicated. Nonnormally distributed data were compared using their median ± absolute deviation

and nonparametric tests [Kolmogorov–Smirnov (KS), unless otherwise indicated]. The precision of single-particle tracking was assessed as described previously (see supplemental material, available at www.jneurosci.org). All statistical operations used Matlab (Mathworks).

## Results

### Astrocytes internalize FM dyes in an activity-independent manner

The incubation at room temperature of cortical astrocytes in saline solution containing 6.7 $\mu$M FM4-64 during 15 min resulted in its uptake into diffraction-limited near-membrane vesicular compartments (Fig. 1*A*) (273 ± 85 nm; mean ± SD; $n$ = 337 puncta) (for details, see supplemental Fig. 2 and Movie S2, available at www.jneurosci.org as supplemental material). We labeled astroglial vesicles with FM4-64 rather than with AO, because AO photoinduced vesicle burst is easily mistaken for exocytotic fusion (Jaiswal et al., 2007) (supplemental Fig. 1 and Movie S1, available at www.jneurosci.org as supplemental material), and FM4-64, unlike AO, can be distinguished from EGFP fluorescence (Nadrigny et al., 2007). The styryl dye was contained in the inner leaflet of the organelle membrane, because disruption of the plasma membrane of FM4-64/OGB-1 double-labeled astrocytes in $Ca^{2+}$-free extracellular solution caused the loss of OGB-1 from the cytoplasm but the retention of FM4-64 spots. The addition to astrocytes incubated in FM1-43 of BPB, a hydrophilic pH indicator and FM1-43 quencher at neutral and mild acid pH (for details, see supplemental material, available at www.jneurosci.org) efficiently deleted the plasma membrane FM1-43 signal, but did not affect FM dye already internalized in vesicular compartments (supplemental Fig. 3, available at www.jneurosci.org as supplemental material).

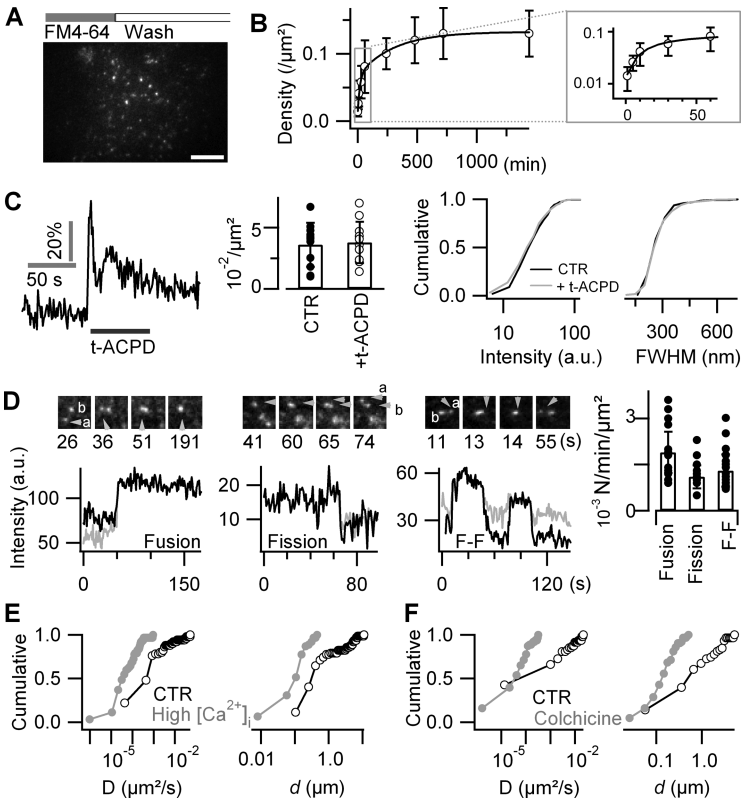


**Figure 1.** Astroglial FM labeling is activity independent. ***A***, A 488 nm evanescent-wave excited fluorescence image of an astrocyte labeled by 15 min incubation in 6.7 $\mu$M FM4-64, followed by 20 min wash. Scale bar, 10 $\mu$m. ***B***, Time-dependent uptake of FM4-64. Varying incubation times from 1 min to 24 h ($n$ = 7–12 cells for each condition) revealed a biexponential increase in spot density. The inset displays zoom on 1–60 min time window. Error bars indicate SD of the mean. ***C***, mGluR activation by perfusing during 5 min 100 $\mu$M t-APCD evoked a $[Ca^{2+}]_i$ increase but did not affect the density, intensity, or size of FM-labeled puncta ($n$ = 7 cells). Error bars indicate SD of the mean. ***D***, Successive fusion and fission events of FM4-64-labeled puncta. Left, As a newcomer vesicle (a) fused with a resident vesicle (b), the fluorescence intensity of the resultant spot increased to the sum of both donor compartments (supplemental Movie S3, available at www.jneurosci.org as supplemental material). Middle, Fission split the initial fluorescence of the donor vesicle (arrowhead) into two dimmer daughter compartments (a and b), which then moved independently (supplemental Movie S4, available at www.jneurosci.org as supplemental material). Right, Fusion–fission (F–F) event of two vesicles (a and b) merging and a third vesicle departing (supplemental Movie S5, available at www.jneurosci.org as supplemental material). Traces were corrected for local background. The gray and black traces are from vesicles a and b, respectively. Scale bar, 2 $\mu$m. Frequency of different types of dynamic interactions among labeled vesicles ($n$ = 14 cells per condition; median ± absolute deviation). ***E***, ***F***, Cumulative histograms of mobility parameters of tracked single FM-labeled spots. Increasing intracellular $[Ca^{2+}]_i$ by controlled mechanical stimulation (***E***, gray) or disruption of microtubules with colchicine (***F***, gray) (100 $\mu$M; 4 h) decreased the average short-range diffusion coefficient, $D$ (left panels), and reduced the displacement, $d$ (right panels), compared with controls (black traces).

FM staining after 15 min incubation at 37°C did not differ from that observed at 25°C. Longer incubations at 37°C enhanced the density of FM4-64-stained puncta in a biphasic manner from 0.01 ± 0.01 $\mu m^{-2}$ at 1 min to 0.13 ± 0.03 $\mu m^{-2}$ after 24 h, with fast (~18 min) and slow (~5 h) components of comparable amplitude (46 vs 54%, respectively) (Fig. 1*B*).

In neurons and neuroendocrine cells, stimulation of exocytosis in the presence of FM4-64 results in an activity-dependent labeling of the freshly added membrane and its subsequent internalization during endocytic recapture (Betz et al., 1992). In contrast, in astrocytes we found that the activation of mGluRs with *trans*-1-aminocyclopentane-1,3-dicarboxylate (t-APCD) (100 $\mu$M; 5 min) triggered $[Ca^{2+}]_i$ elevations with $dF/F_0$ = 37 ± 11% peak amplitude ($n$ = 7 cells; $p$ = 0.49 vs spontaneous $Ca^{2+}$ elevations) but did not significantly change FM4-64 labeling, nor did it affect the density ($n$ = 11 cells per condition; $p$ = 0.86, $t$ test), size ($p$ = 0.48, $t$ test), or intensity ($p$ = 0.44, KS test) of individual FM4-64-labeled puncta ($n$ = 227–368 vesicles from four cells per condition) (Fig. 1*C*).

The high resistance of FM4-64 to photobleaching ($\tau_{bleach}$ = 378 ± 165 s; $n$ = 11) permitted us the visualization of successive fusions and fissions of FM-labeled spots revealing their complex intracellular trafficking (Fig. 1*D*; supplemental Movies S3–S5, available at www.jneurosci.org as supplemental material). Controlled mechanical stimulation (m-Stim)-evoked $[Ca^{2+}]_i$ increases ($dF/F_0$ = 60 ± 29%; $n$ = 12 transients from three cells) reduced both the diffusion coefficient [$D$ = 0.04 ± 0.1 × $10^{-3}$ during elevated $[Ca^{2+}]_i$ vs 0.7 ± 5.0 × $10^{-3}$ $\mu m^2 s^{-1}$ in control (CTR); median ± absolute deviation; $n$ = 62 vesicles from the same cells for each condition; $p < 0.01$] and the displacement $d$, which was 0.12 ± 0.08 $\mu$m during elevated $Ca^{2+}$ (minimum, 0.01 $\mu$m; maximum, 0.46 $\mu$m) versus 0.40 ± 1.6 $\mu$m (minimum, 0.10 $\mu$m; maximum, 11.1 $\mu$m) under CTR conditions (median ± absolute deviation; $p < 0.01$, KS test) (Fig. 1*E*).

To study the involvement of active transport along microtu-

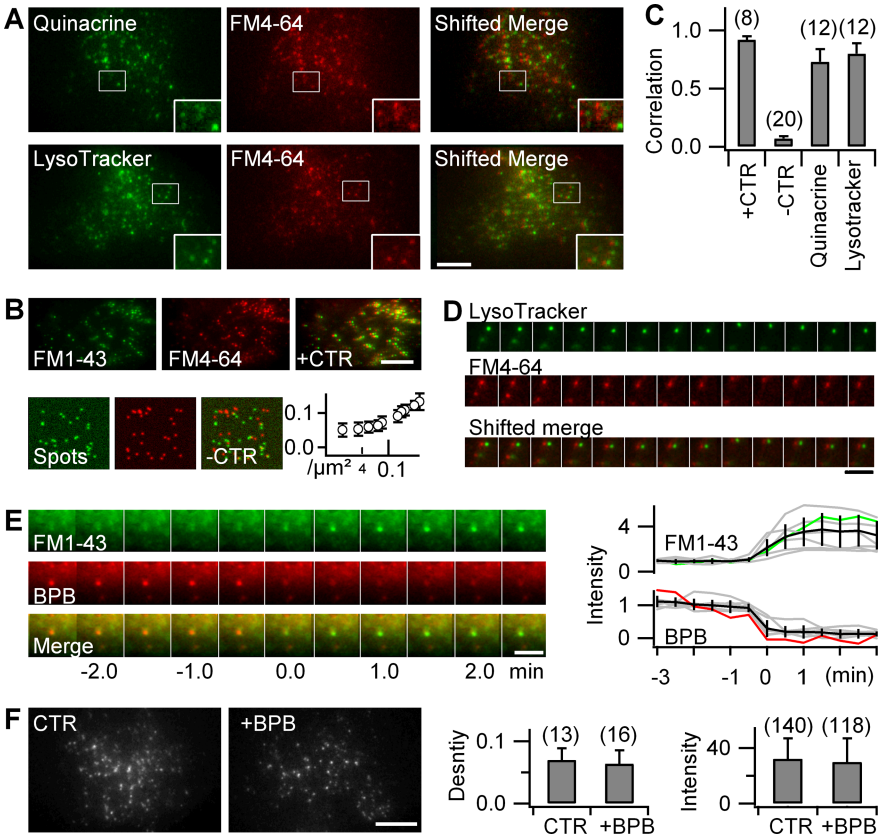


**Figure 2.** FM dyes label all acidic astroglial compartments. ***A***, Dual-color TIRF images of FM4-64-stained astrocytes colabeled with the acidic-compartment markers quinacrine (top) or Lysotracker Green (bottom). The boxed areas are shown at higher magnification (insets). To better visualize colocalization, the red-channel image is left-shifted by 5 pixels relative to the green channel (shifted merge). Scale bar, 10 $\mu$m. ***B***, Quantifying colocalization. Top, Coloading of FM1-43 and FM4-64 (6.7 $\mu$M; 15 min, followed by 20 min wash for both dyes) was used as a positive control (+CTR; $\tilde{r}_{12} = 0.92 \pm 0.03$). Bottom, Computer-generated image pairs containing randomly placed fluorescent spots at the same density as FM-labeled organelles were used as negative controls (−CTR). Spots were blurred with the experimental point-spread function and noise added to mimic the signal-to-noise ratio of typical FM4-64 images. Evolution of false apparent colocalization with particle density. In our imaging conditions (~0.01–0.1 spots/$\mu$m$^2$), $\tilde{r}_{12} = 0.07 \pm 0.02$ (−CTR; $n = 20$ trials) defines the lower bound of useful colocalization estimates. ***C***, Values of $\tilde{r}_{12}$ were significantly different for quinacrine and Lysotracker versus both −CTR and +CTR (Table 1). Numbers are cells examined. Error bars indicate SD of the mean. Scale bar, 10 $\mu$m. ***D***, Object-based colocalization. Dual-color epifluorescence tracking (1 Hz) of Lysotracker and FM4-64 shows the comovement of both labels (shifted merge). Scale bar, 3 $\mu$m. ***E***, BPB reports vesicle acidification. Interlaced dual-excitation dual-emission epifluorescence images of a tracked and recentered single FM1-43/BPB double-labeled vesicle. The traces (right panel) illustrate the concomitant and antiphasic fluorescence changes of FM1-43 (green) and BPB (red) fluorescence for the organelle shown left, as well as for other organelles (gray) that were temporally aligned to the midpoint of the red-to-green transition ($t = 0$ s) and normalized to the pretransition fluorescence, indicating the lifting of FM quenching with time after internalization. The population average is in black. Scale bar, 2 $\mu$m. ***F***, The 488/560 nm (ex/em) TIRF images of an astrocyte labeled by FM1-43 in the absence (CTR) and presence of BPB. BPB uptake did not modify the density ($p = 0.5$, $t$ test) nor the intensity ($p = 0.63$, KS test) of FM1-43-labeled vesicles. Shown are numbers of cells (density) and vesicles (intensity). Scale bar, 10 $\mu$m.

bules in the mobility of FM-labeled spots, astrocytes were imaged under control conditions and after treatment with colchicine (100 $\mu$M; 4 h). Colchicine application compacted vesicle trajectories (for raw data, see supplemental Fig. 4, available at www.jneurosci.org as supplemental material), reducing both the overall mobility by an order of magnitude ($D = 0.05 \pm 0.06 \times 10^{-3}$ in colchicine, $n = 63$ vesicles in four cells; vs $0.68 \pm 3.6 \times 10^{-3}$ $\mu$m$^2$s$^{-1}$ in CTR, $n = 58$ vesicles in three cells; median ± absolute deviation; $p < 0.001$, KS test), and reducing the displacement from the initial location to the point reached 60 s thereafter by a factor of ~4 ($d = 0.15 \pm 0.08$ $\mu$m in colchicine; minimum, 0.03 $\mu$m, maximum, 0.51 $\mu$m; vs $0.62 \pm 1.0$ $\mu$m in CTR; minimum, 0.06 $\mu$m, maximum, 5.4 $\mu$m; median ± absolute deviation; $p <$ 0.001, KS test) (Fig. 1*F*).

In conclusion, short exposure of astrocytes to micromolar concentrations of styryl dyes led to their uptake into near-diffraction limited vesicular organelles that could be tracked over tens of minutes. This uptake was activity independent.

### FM dyes label all acidic vesicles in astrocytes

FM-labeled puncta potentially represent a diversity of organelles including endocytic and exocytic vesicles, endosomal and lysosomal compartments, as well as transport vesicles. Surprisingly, labeling astrocytes with the weak bases quinacrine or Lysotracker Green resulted in a yellow/green punctate staining that almost completely overlapped with FM4-64 on dual-color TIRF images (Fig. 2*A*). We quantified the amount of colocalization by first verifying the absence of spectral cross talk between acidic-compartment markers and FM4-64 (supplemental Fig. 5, available at www.jneurosci.org as supplemental material), and then calculating a noise-corrected Pearson's correlation coefficient, $\tilde{r}_{12}$ (Table 1).

The labeling resulting from both acidic-vesicle markers highly correlated with FM4-64, with $\tilde{r}_{12}$ values close to the positive control value obtained from FM1-43/FM4-64 double-labeled astrocytes (Fig. 2*B*,*C*) (see also supplemental material, available at www.jneurosci.org). The observation that both Lysotracker and FM4-64 systematically moved together on time-lapse epifluorescence images (Fig. 2*D*) confirmed the colocalization between FM4-64 and Lysotracker Green.

Perhaps the few FM4-64-stained organelles not labeled by quinacrine or Lysotracker Green were freshly formed and not yet acidic enough to accumulate these acidotropic dyes. By quenching FM1-43 fluorescence at neutral and mild acid pH but not at low pH values ($pK_a \sim 4.0$), BPB imprints its pH dependence on the FM1-43 signal (Harata et al., 2006; Zhang et al., 2007). Coapplication of both dyes resulted in their simultaneous uptake into single vesicular organelles, for some of which we could visualize the red-to-green transition from BPB to FM1-43 emission (Fig. 2*E*), indicating the lifting of FM1-43 quenching after the acidification of the organelle lumen. Examination of BPB/FM1-43 double-labeled cells 1–3 h later demonstrated a density and intensity of FM labeling that was indistinguishable from control astrocytes labeled only with FM1-43 (Fig. 2*F*), showing that the intraluminal pH of FM1-43/BPB double-labeled organelles was now too low for BPB to quench FM fluorescence. Single-vesicle spectral imaging (Nadrigny et al., 2006) confirmed the presence of both dyes (supplemental Fig. 3, available at www.jneurosci.org as supplemental material).

**Table 1. Values of modified Pearson's correlation coefficient of FM4-64 pixels versus acidic organelle and fluorescent protein markers**

| | $\tilde{r}_{12}$ | *n* | *p* value[a] | Compartment labeled |
|---|---|---|---|---|
| FM1-43 | 0.92 ± 0.03 | 8 | ND | FM-labeled compartments |
| Quinacrine | 0.79 ± 0.07 | 12 | ND | Acidic vesicles |
| Lysotracker Green | 0.84 ± 0.09 | 12 | ND | Acidic vesicles |
| BPB | 0.58 ± 0.10 | 9 | ND | |
| EGFP-sialin | 0.83 ± 0.09 | 11 | ND | Lysosomes/late endosomes (Morin et al., 2004) |
| CD63/LAMP3-EGFP | 0.68 ± 0.19 | 12 | | Lysosomes/late endosomes |
| Ti-VAMP/VAMP7-EGFP | 0.74 ± 0.13 | 9 | ND | Lysosomes/late endosomes (Advani et al., 1999; Martinez-Arca et al., 2000) |
| VAMP8-EGFP | 0.55 ± 0.17 | 24 | <0.05 | Early and late endosomes (Metzelaar et al., 1991; Martinez-Arca et al., 2000) |
| VAMP2-EGFP | 0.39 ± 0.18 | 23 | <0.001 | Small secretory vesicles (Parpura et al., 1995) |
| VAMP3-EGFP | 0.38 ± 0.23 | 20 | <0.001 | Early endosomes/intermediate transport vesicles (Chilcote et al., 1995; Teter et al., 1998) |
| VGlut1-Venus[b] | 0.31 ± 0.17 | 14 | <0.001 | Glutamate-containing synaptic-like microvesicles (Wojcik et al., 2004) |
| VGlut3-Venus[b] | 0.27 ± 0.22 | 14 | <0.001 | Glutamate-containing synaptic-like microvesicles (Seal and Edwards, 2006) |
| Computer-generated image | 0.07 ± 0.02 | 20 | ND | Absence of colocalization |

$\tilde{r}_{12}$, Noise-reduced modified Pearson's coefficient (see supplemental material, available at www.jneurosci.org); *n*, number of cells (or trials).

[a]Significance of difference versus $\tilde{r}_{12}$ value of CD63-EGFP.

[b]For additional explanation of these two markers, see supplemental Figure 9 (available at www.jneurosci.org as supplemental material).

Our results so far indicate that FM4-64 labels most acidic vesicles present in astroglia and that these organelles have a low luminal pH. This, together with the colocalization between FM4-64 and the LysoTracker, raises the possibility that these vesicles are lysosomes.

### FM mainly labels astroglial late endosomal/lysosomal compartments

To further characterize the FM4-64-labeled organelles, we expressed various vesicular proteins fused to yellow-green fluorescing proteins and performed a comparative analysis of their correlation with FM4-64-labeled pixels on dual-color evanescent-field images. We observed the highest degree of correlation between FM4-64 and EGFP staining when the latter was linked to the lysosomal transporter sialin (for $\tilde{r}_{12}$ values, see Table 1). A strong correlation was also found between FM4-64 and two other EGFP-tagged late endosomal/lysosomal membrane proteins, CD63/LAMP3, and the toxin-insensitive vesicular-soluble *N*-ethylmaleimide-sensitive factor attachment protein receptor (v-SNARE) Ti-VAMP/VAMP7 (Fig. 3*A*). The correlation was relatively smaller for endobrevin/VAMP8, mediating the intracellular trafficking between endosomes and lysosomes, and for the ubiquitously expressed v-SNARE cellubrevin/VAMP3, a marker for endosome-derived astroglial vesicles, as well as the synaptic-like vesicle marker VAMP2 (Fig. 3*B*). The lowest correlation was observed between FM4-64 and either VGlut1- or VGlut3-Venus constructs (Fig. 3*C*) (see additional details in supplemental Fig. 9, available at www.jneurosci.org as supplemental material). The results summarized in Figure 3*D* indicate that FM4-64 labels mainly late endosomal/lysosomal compartments.

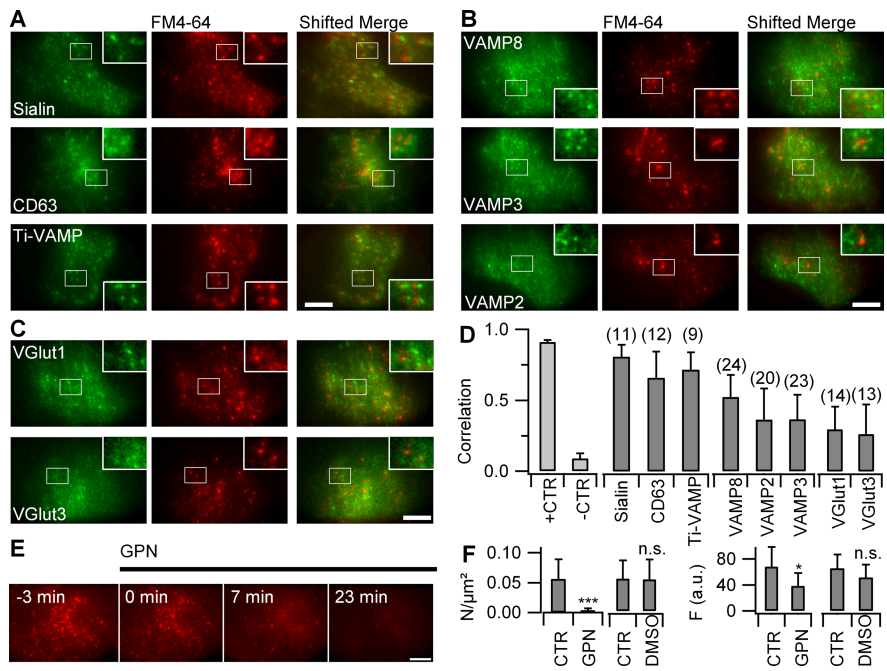


**Figure 3.** FM-labeled vesicles are late endosomes/lysosomes. ***A***, TIRF images of astrocytes expressing EGFP-sialin (top), CD63/LAMP3 (middle), and Ti-VAMP (bottom), labeled with FM4-64. The insets show boxed regions at higher magnification. Color-merged images (shifted merge) as in Figure 2 are shown. ***B***, Expression of EGFP-VAMP8 (top), EGFP-VAMP3 (middle), and VAMP2 (bottom). ***C***, Venus-VGlut1 and -3 labeling. ***D***, Modified Pearson's correlation coefficient $\tilde{r}_{12}$ between FM4-64 and various organelle markers (see supplemental material, available at www.jneurosci.org). Number of cells analyzed indicated above bars. Error bars indicate SD of the mean. ***E***, Time-lapse epifluorescence images of a FM4-64-labeled astrocyte before (−3 min) and after selective lysosomal lysis with GPN (200 μM). ***F***, Density of FM-labeled puncta (left) and whole-cell fluorescence intensity (right) for control and GPN-treated astrocytes, imaged 30–60 min after application of 200 μM GPN ($n = 7$–15). The same dilution (1:500) of DMSO had no effect on the stability of FM-loaded organelles ($n = 4$ cells). Scale bars, 10 μm. *$p < 0.05$; ***$p < 0.001$.

To further substantiate the identification of FM-labeled vesicles as lysosomes, independently of protein expression, we applied glycyl-L-phenylalanine 2-naphthylamide (GPN), a cathepsin-C substrate that causes lysosome lysis in astrocytes

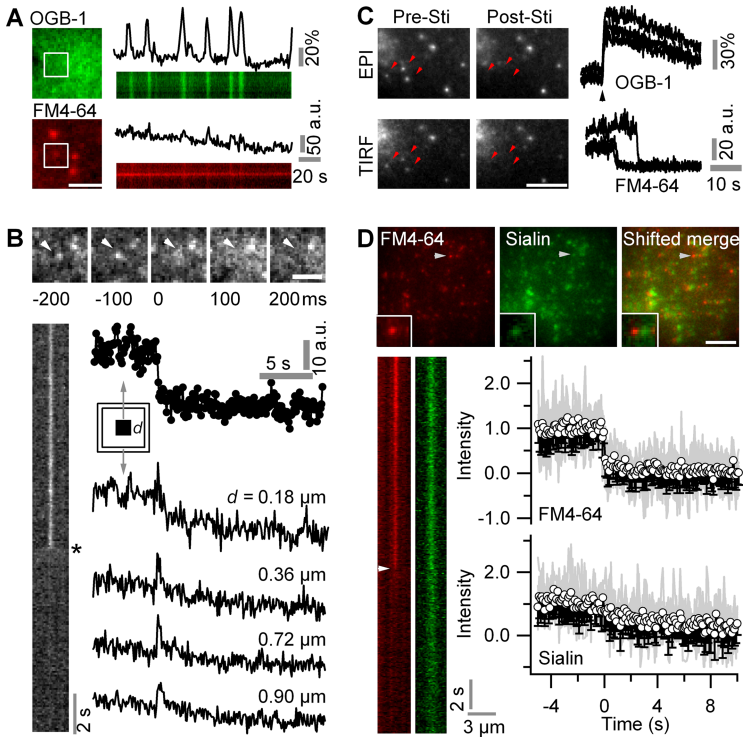


**Figure 4.** Astroglial lysosomes undergo $Ca^{2+}$-dependent complete exocytosis. ***A***, Spontaneous $Ca^{2+}$ oscillations did not trigger exocytosis of FM4-64-labeled puncta ($n = 92$ $Ca^{2+}$ transients in 12 cells). Scale bar, 3 $\mu$m. ***B***, Typical signature of a fusion event in response to m-Stim on sequential TIRF images of a 488 nm excited 10 Hz ministack and kymograph. The central FM4-64-loaded vesicle (arrowhead) fuses at a time 0. Note the rapid destaining and spread of FM4-64 fluorescence (asterisk). Right, Fluorescence changes with time, measured in a small subregion centered on the same vesicle (3 × 3 pixels; circles) and in several concentric regions (0.2 $\mu$m wide) with increasing distance *d*. Scale bar, 2 $\mu$m. ***C***, Left, Epifluorescence (EPI) and TIRF images of the same region of an FM4-64-labeled astrocyte before (Pre-Sti) and after (Post-Sti) stimulation. Epifluorescence FM4-64 and TIRF OGB-1 fluorescence from 1 × 1 $\mu$m single-spot regions in response to m-Stim (black arrowhead). Systematic and simultaneous $Ca^{2+}$-dependent loss of the vesicle from EPI and TIRF images (supplemental Movie S6, available at www.jneurosci.org as supplemental material) indicates dye release in the extracellular space and not movement from the evanescent field into deeper cytoplasmic regions. Scale bar, 5 $\mu$m. ***D***, Top, Dual-color 488-nm TIRF images of a EGFP-sialin/FM4-64 double-labeled astrocyte. Inset, Zoom near arrowhead. Bottom, Kymographs of the same vesicle (10 Hz) undergoing exocytosis in response to m-Stim (supplemental Movie S7, available at www.jneurosci.org as supplemental material). The white arrowhead identifies FM4-64 release at $t = 0$ s. The initiation of exocytosis was defined as the first point of FM4-64 fluorescence falling below the 2 s prestimulus average minus three times its SD. Evolution with time of FM4-64 (top) and EGFP (bottom) fluorescence of $n = 13$ double-labeled organelles undergoing $Ca^{2+}$ triggered exocytosis after m-Stim. The gray traces are superimposed individual normalized and temporally aligned events. The traces were corrected for local background. Scale bar, 10 $\mu$m.

(Zhang et al., 2007) and other cell types, probably as a result of its intraluminal hydrolysis in lysosomes. In line with the strong overlap between established lysosomal markers and FM4-64, the addition of GPN (200 $\mu$M) to the perfusion medium abolished FM4-64 punctate labeling within minutes (Fig. 3*E*) and produced a diffuse fluorescence throughout the cell at later times (supplemental Fig. 6, available at www.jneurosci.org as supplemental material). This cytoplasmic relocation was not attributable to solvent action because DMSO alone had no effect (Fig. 3*F*). Global cell damage was excluded by the observation of evoked calcium transients in cells treated with GPN (supplemental Fig. 6, available at www.jneurosci.org as supplemental material).

Together, the high correlation between three established late endosomal/lysosomal fluorescent markers and FM labeling, as well as the loss of FM-labeled organelles after selective lysosomal disruption confirms that styryl dyes predominantly label late endosomes/lysosomes in cultured cortical astrocytes.

### Submicromolar $[Ca^{2+}]_i$ triggers complete lysosome fusion

Cultured astrocytes loaded with OGB-1 displayed spontaneous $[Ca^{2+}]_i$ transients ($dF/F_0 = 40 \pm 13\%$; $n = 12$ cells) that systematically failed to trigger the release of FM4-64 spots (Fig. 4*A*). Performing experiments at 37°C increased the frequency of spontaneous $[Ca^{2+}]_i$ transients without changing their amplitude nor affecting FM labeling (data not shown). Activation of mGluRs by t-ACPD (100 $\mu$M; 60–120 s) systematically evoked calcium transients but failed to trigger exocytosis in all 16 cells examined. A recent study has identified a close link between mechanosensitive TRPC (transient receptor potential type-C) store-operated channels (SOCs) and ER $Ca^{2+}$ stores (Golovina, 2005). Therefore, we delivered minimal mechanical stimuli of controlled amplitude (m-Stim) with a piezo-controlled patch pipette (for controls, see supplemental Fig. 7, available at www.jneurosci.org as supplemental material). Among 91 cells without membrane rupture, 82 responded with $Ca^{2+}$ elevations. Evoked $Ca^{2+}$ elevations ($dF/F_0 = 59 \pm 11\%$) triggered exocytosis of 5.3 ± 3.2 FM4-64-labeled spots ($n = 72$) per astrocyte footprint (884 ± 128 $\mu m^2$) in 16 of 82 cells, corresponding to the release of a 4.9 ± 2.4% subpopulation of FM-labeled puncta. This proportion did not increase when performing experiments at 37°C ($n = 10$ cells) (data not shown).

At the single-organelle level, m-Stim triggered submicromolar $Ca^{2+}$ elevations that evoked the loss of FM4-64 fluorescence in a small 0.6 $\mu$m × 0.6 $\mu$m region of interest (ROI) centered on the fluorescent spot, along with the spread of fluorescence into the periphery. This cloud of released FM molecules is seen on the kymograph as a fading tossed Y-shaped profile of evanescent-field excited FM4-64 fluorescence (Fig. 4*B*). $Ca^{2+}$-triggered single secretory events seen on TIRF images (supplemental Movie S6, available at www.jneurosci.org as supplemental material) were always accompanied by the simultaneous loss of spots on interleaved epifluorescence images, indicating that the loss of FM fluorescence is attributable to the extracellular release of dye rather than its intracellular relocation ($n = 20$ cells) (Fig. 4*C*, example traces).

Several studies (Chen et al., 2005; Bowser and Khakh, 2007; Zhang et al., 2007) suggested that astrocytes could make efficient use of their limited pool of secretory vesicles by using a "kiss-and-run" mechanism of gliotransmitter release. We therefore measured, for each spot individually, the evanescent-field excited fluorescence intensity after the subtraction of the local background ($B_{loc}$). Values of $B_{loc}$ varied considerably from one spot to another [126.3 ± 126.9 counts per second (cps); median ± absolute deviation; minimum, 80.1 cps; maximum, 722.1 cps; $n = 35$ regions] and systematically decreased on m-Stim. The subtraction of the time-varying $B_{loc}$ resulted in the complete loss of FM fluorescence from the organelle after membrane fusion, illustrating the absence of partial destaining. Subtraction of the average extracellular background instead, however, produced apparent

partial destaining events (supplemental Fig. 8, available at www.jneurosci.org as supplemental material). Full-fusion events were also observed with FM2-10, a dye that more rapidly dissociates from lipid membranes than do FM1-43 or FM4-64 (supplemental Fig. 8, available at www.jneurosci.org as supplemental material).

Although our observation of the complete loss of FM fluorescence (Fig. 4*B*) is not in favor of a partial release mechanism, it does not exclude that the vesicle stays on the plasma membrane and is refilled for another round of rapid exocytosis after the loss of FM4-64. Thus, to study the postfusion fate of lysosomes, we monitored, in triple-labeled astrocytes expressing an EGFP-sialin construct, the evolution with time of FM4-64 and EGFP fluorescence of individual double-labeled spots after m-Stim (supplemental Movie S7, available at www.jneurosci.org as supplemental material). At the same time, interlaced 568 nm evanescent field excitation of the red emitting $Ca^{2+}$ indicator X-rhod-1 permitted the detection of the local $Ca^{2+}$ signal at the site of exocytosis (supplemental Fig. 5, available at www.jneurosci.org as supplemental material). Whereas the FM4-64 signal was lost instantly for all 72 destaining events, as expected from the ~300-fold decrease in quantum yield of the styryl dye on departitioning into the aqueous phase, the EGFP signal dissipated on average much slower ($\tau = 3.7 \pm 1.5$ s; monoexponential fit ± 95% confidence interval) (Fig. 4*D*). The complete loss of EGFP fluorescence is compatible with the slow diffusion of sialin after the establishment of lipid continuity and eventually complete fusion of lysosomal and plasma membranes. The same experiment was performed in cells transfected with VGlut fusion proteins. Among 57 destaining events evoked by m-Stim (32 and 25 events from six VGlut1- and four VGlut3-expressing cells, respectively), only two events were detected from VGlut-positive organelles (3.5%) (supplemental Fig. 9, available at www.jneurosci.org as supplemental material). The time course of the destaining of VGlut-positive organelles was not measurably different from that observed for sialin–EGFP-expressing lysosomes, confirming the complete insertion of vesicular organelles in the plasma membrane.

In summary, whereas spontaneous $Ca^{2+}$ waves failed to trigger exocytosis, mechanically evoked submicromolar $Ca^{2+}$ transients evoked the full-blown fusion of late endosomal/lysosomal compartments from cultured astrocytes that led to a loss of the organelle identity after fusion.

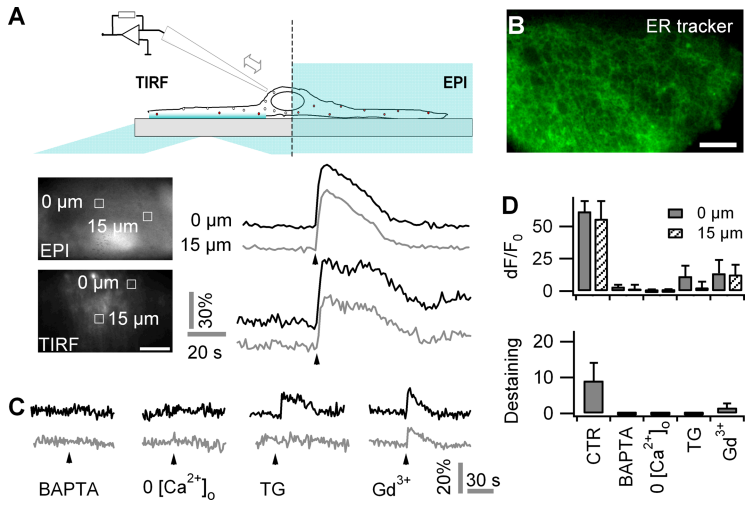


**Figure 5.** Mechanically evoked astroglial exocytosis requires both extracellular and intracellular store-operated $Ca^{2+}$. ***A***, Top, Scheme of combined TIRF and epifluorescence (EPI) imaging of near-membrane and bulk $[Ca^{2+}]_i$ in response to m-Stim. Bottom, Typical EPI and TIRF images of OGB-1-labeled astrocyte, and temporal profiles of the $Ca^{2+}$ response ($dF/F_0$) to m-Stim (arrowhead) at the stimulation site (black) and 15 $\mu$m apart (gray); ROIs are identified on the images nearby. ***B***, Subcellular distribution of ER tracker (EPI). Scale bars, 10 $\mu$m. ***C***, Representative traces of evoked $Ca^{2+}$ responses to m-Stim from BAPTA, AM-treated astrocytes (60 $\mu$M, 40 min; left), $Ca^{2+}$-free extracellular solution (middle left), thapsigargin (TG) (500 nM, 30 min; middle), and $Gd^{3+}$ (100 $\mu$M; middle right). ***D***, Average $dF/F_0$ peak amplitudes of $Ca^{2+}$ responses at the site of m-Stim (solid bars) and 15 $\mu$m apart (hatched) as well as numbers fusion events per cell in the same conditions. Error bars indicate SD of the mean.

## Exocytosis requires both extracellular $Ca^{2+}$ and mobilization of $Ca^{2+}$ from intracellular stores

The lack of lysosomal exocytosis in response to spontaneous $[Ca^{2+}]_i$ transients comes as a surprise because both the spontaneous (Nett et al., 2002; Parri and Crunelli, 2003) and evoked (Araque et al., 1998; Hua et al., 2004) $Ca^{2+}$ signals are similar in amplitude and involve the mobilization of $Ca^{2+}$ from ER $Ca^{2+}$ stores. We therefore studied the sources of $Ca^{2+}$ contributing to the $[Ca^{2+}]_i$ transient evoked by m-Stim. Evoked $Ca^{2+}$ signals had temporal profiles and peak amplitudes that were indistinguishable in the near-membrane and cytoplasmic compartments ($dF/F_0 = 64 \pm 1\%$, $n = 42$ transients from eight cells for TIRF, vs $dF/F_0 = 62 \pm 8\%$, $n = 72$ transients from eight cells for epifluorescence; *t* test, $p = 0.28$) (Fig. 5*A*). A rise in $[Ca^{2+}]_i$ occurred within 1 s throughout the astrocyte with no measurable attenuation in peak amplitude or slowdown of kinetics over a 15 $\mu$m distance. Near-membrane $dF/F_0$ $Ca^{2+}$ measured in the same cell in 1 × 1 $\mu$m regions centered on fusion sites was not significantly different from those at spots not undergoing exocytosis (64 ± 10%, $n = 42$, vs 62 ± 10%, $n = 45$; $p = 0.32$). These results suggest that the intracellular $Ca^{2+}$ signal propagates regeneratively rather than by passive diffusion through the cytoplasm where an attenuation and slowdown caused by $Ca^{2+}$ buffering would be expected. Indeed, ER Tracker labeling showed a dense meshwork that stretched out through the entire astrocyte, compatible with the idea of a rapid and unbuffered diffusion and equilibration of $Ca^{2+}$ within the continuous ER and subsequent release of $Ca^{2+}$ into the cytoplasm (Hua et al., 2004; Golovina, 2005) (Fig. 5*B*).

A pharmacological dissection of the sources of $Ca^{2+}$ showed that m-Stim evoked lysosomal exocytosis required both intracellular and extracellular $Ca^{2+}$ (Fig. 5*C*). Chelating intracellular $Ca^{2+}$ with 60 $\mu$M BAPTA-AM abolished both evoked $Ca^{2+}$ transients ($dF/F_0 = 3 \pm 2\%$) and exocytosis (zero events in nine treated cells vs 9.1 ± 5.0 events/cell, on average, under control). Likewise, the omission of $Ca^{2+}$ from and addition of 2 mM EGTA to the extracellular fluid impaired both evoked $[Ca^{2+}]_i$ increases ($dF/F_0 = 0 \pm 1\%$; $n = 9$ cells) (for experimental details, see supplemental Fig. 10, available at www.jneurosci.org as supplemental material) and secretion (Fig. 5*D*).

Astroglial lysosomal exocytosis can persist in the absence of mechanically gated $Ca^{2+}$ entry, because 100 $\mu$M $Gd^{3+}$ affected only partially both the $Ca^{2+}$ signal ($dF/F_0 = 14 \pm 10\%$; 22% of CTR; $n = 9$ cells) and exocytosis (1.6 ± 1.2 events; 18% of CTR) evoked by m-Stim. When blocking $Ca^{2+}$ store replenishment with 500 nM thapsigargin, m-Stim provoked a reduced $Ca^{2+}$ response ($dF/F_0 = 12 \pm 8\%$; 19% of CTR; $n = 8$ cells) that failed to

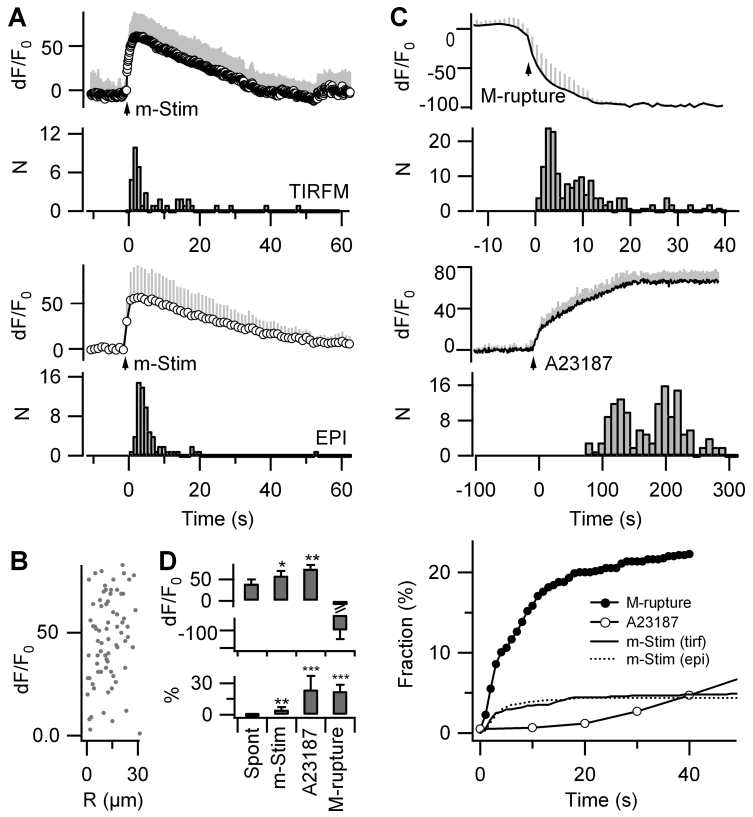


**Figure 6.** $Ca^{2+}$-triggered asynchronous exocytosis of a subset of lysosomes. ***A***, $Ca^{2+}$ traces and temporal distribution of FM destaining pooled from $n = 8$ OGB-1/FM4-64 double-labeled astrocytes, imaged with 10 Hz 488 nm TIRF (top) and 1 Hz 488 nm epifluorescence excitation (bottom). Traces were aligned to the first $Ca^{2+}$ data point reaching 63% of the peak $dF/F_0$ value and normalized by the 5 s (TIRF) or 20 s (EPI) prestimulus fluorescence and finally averaged. The time course of FM destaining measured in TIRF (top; 42 events) and epifluorescence (bottom; 72 events; $p = 0.6$, KS test) did not significantly differ and occurred several seconds after the peak $[Ca^{2+}]_i$. ***B***, Parametric plot of $dF/F_0$ $Ca^{2+}$ versus distance $R$ from the site of m-Stim shows no correlation ($n = 72$ fusion events). ***C***, Top, Instantaneous $[Ca^{2+}]_i$ increases after membrane rupture detected as the loss of OGB-1 fluorescence resulted in the rapid release of the entire RRP. Middle, Application of the $Ca^{2+}$ ionophore A-23187 (50 $\mu$M) in the presence of 2 mM extracellular $Ca^{2+}$ gradually increased $Ca^{2+}$ to a maximum of $dF/F_0 = 75 \pm 10\%$. Exocytosis required 0.5 $dF/F_0$ $Ca^{2+}$ to start ($n = 4$ cells; inset) and reached an amplitude four times larger than that observed with m-Stim (9.1 ± 5.0 vs 39.0 ± 23.5 fusion events/cell). Bottom, Comparison of the release kinetics for m-Stim, ionophore, and membrane rupture. ***D***, Peak $[Ca^{2+}]_i$ $dF/F_0$ and percentage of FM-labeled vesicles released under various conditions ($n = 6$–9 cells each). Differences versus spontaneously occurring $[Ca^{2+}]_i$ transients. Error bars indicate SD of the mean. *$p < 0.05$; **$p < 0.01$; ***$p < 0.001$.

trigger membrane fusion. The nonspecific $Ca^{2+}$-permeable channel blocker $Gd^{3+}$ similarly affected both the local and distant $[Ca^{2+}]_i$ as well as exocytosis. In contrast, thapsigargin abolished predominantly the propagated $[Ca^{2+}]_i$ elevation, indicating that the activation of mechanosensitive channels creates a local $Ca^{2+}$ domain that is insufficient to trigger exocytosis but becomes a trigger for lysosomal exocytosis when amplified by $Ca^{2+}$ release from the ER, probably through a $[Ca^{2+}]_i$ induced $Ca^{2+}$ release (CICR) mechanism. In keeping with this idea, the cumulative effect on $Ca^{2+}$ and exocytosis of mechanically gated $Ca^{2+}$ influx and mobilization of $Ca^{2+}$ from the ER was larger than the sum of the individual components (Fig. 5*D*), suggesting the involvement of CICR and/or secondary $Ca^{2+}$ influx through SOCs.

In summary, our experiments demonstrate that astroglial lysosomal exocytosis is triggered by the influx of extracellular $Ca^{2+}$ through mechanically activated $Gd^{3+}$-sensitive channels and that it requires $Ca^{2+}$ release from the ER. Our observation that $Gd^{3+}$ was a less potent inhibitor of both $[Ca^{2+}]_i$ increases and exocytic responses than was zero extracellular $Ca^{2+}$ suggests the additional presence of a $Gd^{3+}$-insensitive path for $Ca^{2+}$ entry. m-Stim provides a convenient means to produce a uniform $[Ca^{2+}]_i$ elevation throughout the cell and can be delivered at a precise time.

### In response to m-Stim, a subset of lysosomes undergoes asynchronous fusion

In addition to affecting only a small percentage of FM4-64-labeled organelles, fusion events occurred with latencies on the order of seconds after m-Stim ($\Delta t = 3.5 \pm 7.6$ s, median ± absolute deviation; $n = 42$ fusion events). Most (~60%) exocytosis occurred later than 2 s after the $[Ca^{2+}]_i$ peak, during the return of $[Ca^{2+}]_i$ to baseline. Similar observations were made with epifluorescence (72 fusion events in eight cells), thereby excluding a systematic TIRF bias from fusion events at the adherent bottom face of the astrocytes (Fig. 6*A*).

The parametric plot of $dF/F_0$ $Ca^{2+}$ at the moment of exocytosis versus the distance $R$ between the stimulation and fusion sites (Fig. 6*B*) showed no correlation, corroborating our previous finding (Fig. 5) that lysosomes throughout the cell are exposed to $[Ca^{2+}]_i$ high enough to trigger their fusion. Thus, the different latencies of individual fusion events represent rather organelle-to-organelle variability than local $[Ca^{2+}]_i$ variations.

The paucity of fusion events and their sluggish coupling to mechanically evoked intracellular $Ca^{2+}$ elevations could either be attributable to their low fusion probability or a small readily releasable pool (RRP) of lysosomes. To estimate the RRP size, we elicited an instantaneous $Ca^{2+}$ rise by rupturing the membrane with a patch pipette (Fig. 6*C*). This maintained stimulus provoked four to five times more lysosomal fusion than m-Stim (22.3 ± 6.1% of the FM-labeled spots; $n = 4$ cells) with a similar kinetics. We observed a comparable released fraction in response to membrane permeabilization with the $Ca^{2+}$ ionophore A-23187 (Fig. 6*D*), in the presence of 2 mM extracellular $Ca^{2+}$ (24 ± 13% of the total FM-labeled population; $n = 4$ cells). Gradual insertion of the ionophore into the membrane caused a $[Ca^{2+}]_i$ ramp that reached a peak value of $dF/F_0 = 75 \pm 10\%$, $n = 4$ cells. $Ca^{2+}$-triggered exocytosis occurred only after $dF/F_0$ $Ca^{2+}$ had reached $dF/F_0 = 50\%$ and continued at a low rate until the entire RRP was emptied. RRP size was not altered by the previous activation of G-protein-coupled receptors or by spontaneous calcium oscillations suggesting that these $Ca^{2+}$ signals do not affect lysosome priming (supplemental Fig. 11, available at www.jneurosci.org as supplemental material).

In conclusion, functional diversity exists among lysosomes in cortical astrocytes, a subset of which is specialized for $Ca^{2+}$-regulated exocytosis.

## Discussion

Our results demonstrate an unexpected and significant contribution of secretory lysosomes to $Ca^{2+}$-regulated exocytosis from

cortical astrocytes in response to submicromolar $[Ca^{2+}]_i$ elevations likely to be encountered by astrocytes under physiological conditions. However, not all $Ca^{2+}$ transients were equally effective to trigger exocytosis. Only a subset of specialized lysosomes responded in a $Ca^{2+}$-dependent manner and the stimulus–secretion coupling was loose compared with that found in neurosecretory cells. $Ca^{2+}$-dependent exocytosis, traditionally considered a hallmark of specialized secretory cells, is being recognized as a ubiquitous process present in many cell types (Chavez et al., 1996; Coorssen et al., 1996; Ninomiya et al., 1996). We now show that, in astrocytes, as in other "nonprofessional" secretory cells, 10–20% of lysosome-like organelles assume the role of secretory vesicles (Andrews, 2000; Luzio et al., 2007) and undergo $Ca^{2+}$-regulated exocytosis.

**FM uptake into astrocytes is not activity dependent**

Cultured mouse cortical astrocytes take up FM dyes in vesicular organelles, which appeared diffraction-limited and smaller than those reported (Chen et al., 2005; Zhang et al., 2007). It has been proposed that astrocytes take up styryl dyes via endocytosis (Zhang et al., 2007). Our study reveals a spontaneous and activity-independent FM uptake that was unanticipated in view of the mechanism of internalization in neurons (Betz et al., 1992). Nonendocytic FM labeling has also been reported for inner ear hair cells (Nishikawa and Sasaki, 1996; Rouze and Schwartz, 1998; Gale et al., 2001; Meyers et al., 2003), where FM is thought to permeate through mechanotransduction channels.

In neurons, FM selectively labels active nerve terminals, whereas astrocytic FM-labeled vesicles were not associated with any obvious morphological specializations. In neurons, the labeled subpopulation of actively cycling synaptic vesicles can be augmented by increasing the intensity of stimulation during exposure to FM dyes. In contrast, astroglial FM labeling is activity independent and FM redistributes from one organelle to another by successive fusions and fissions, labeling within tens of minutes most acidic vesicular compartments.

**FM selectively labels lysosomes in astrocytes**

The exact nature of the vesicular compartment involved in $Ca^{2+}$-dependent release from astrocytes is a subject of discussion (Coco et al., 2003; Bezzi et al., 2004; Jaiswal et al., 2007; Pangrsic et al., 2007; Zhang et al., 2007). Based on a quantitative correlation of multicolor fluorescence as well as functional arguments, we identify the organelles involved in $Ca^{2+}$-regulated exocytosis as late endosomes/lysosomes, thereby corroborating the observation of Zhang and coworkers (Zhang et al., 2007) who, based on immunolabeling and confocal microscopy, reported a similarly high colocalization between different FM probes and antibodies against lysosomal proteins and a lower degree of overlap between FM and endosome or secretory-vesicle markers. The similar colocalization profiles found by immunostaining and transfection reinforce our interpretation that organelles carrying the transfected fluorescent marker identify the same organelles as those expressing the endogenous nonfluorescent protein. We cannot exclude that protein overexpression drives specific markers onto a lysosomal route for degradation. This possibility is suggested by the lower colocalization estimate between FM and antibody-labeled VGlut1 and VGlut2 (Zhang et al., 2007) compared with the expression of VGlut constructs in our study. A partial mistargeting of alien proteins would also be in line with our previous observation that approximately one-quarter of astroglial lysosomes express the nonlysosomal v-SNARE after transfection of a VAMP2-citrine construct (Nadrigny et al., 2006). However, the possible false-positive labeling of lysosomes as secretory vesicles does not disqualify the use of fluorescent protein chimeras of the lysosomal markers sialin, CD63/LAMP3, and Ti-VAMP/VAMP7. Indeed, our identification of FM-labeled compartments as lysosomes is confirmed independently by using BBP dequenching and GPN-induced lysis (Zhang et al., 2007). Together, our experiments support the surprising conclusion that FM is a selective lysosomal marker in cortical astrocytes.

It might be argued that we miss a subpopulation of vesicles not labeled by FM. This vesicle population, even small, might undergo $Ca^{2+}$-dependent exocytosis and be responsible for gliotransmitter release. In such a case, these compartments should be engaged in exocytic and endocytic vesicle cycling and hence be labeled by FM in an activity-dependent manner, which was not observed, because the activation of mGluRs with the broadband agonist t-APCD failed to affect FM labeling. Hence our findings exclude the presence of a hidden population of astroglial vesicular compartments competent for $Ca^{2+}$-dependent exocytosis.

**Astroglial exocytosis is loosely coupled to near-membrane $[Ca^{2+}]_i$**

In neurons and neuroendocrine cells, voltage-gated $Ca^{2+}$ influx sets up steep near-membrane $[Ca^{2+}]_i$ gradients that trigger synchronous exocytosis. The observed asynchrony between astroglial $Ca^{2+}$ transients and lysosomal secretion argues against a tight coupling between rapid $[Ca^{2+}]_i$ signals and exocytosis and suggests that astrocytes show more resemblance to nonspecialized secretory cells than to fast transmitter release in neurons and neuroendocrine cells. Several nonexclusive explanations could account for the sluggish stimulus–secretion coupling: (1) lysosomal release sites are systematically distant from localized domains of elevated $[Ca^{2+}]_i$, (2) such $Ca^{2+}$ microdomains are absent in astrocytes, (3) the molecular machinery mediating astroglial fusion is intrinsically slow, and (4) prolonged high $[Ca^{2+}]_i$ levels are required for exocytosis.

We have, at present, no experimental support for the presence of $Ca^{2+}$ microdomains, but, in contrast, we have good reasons to believe that the molecular exocytic machinery is intrinsically slow, because maximally stimulating exocytosis at millimolar $[Ca^{2+}]_i$ after membrane rupture accelerated only marginally the exocytic response. This indicates that astrocytic secretion, like lysosomal exocytosis in other cells (Jaiswal et al., 2004), does not operate on a millisecond timescale as suggested previously (Bezzi et al., 2004; Kreft et al., 2004). Also, our findings are compatible with the slow $Ca^{2+}$-dependent assembly of a lysosomal core complex (Rao et al., 2004) composed of SNAP-23, syntaxin 4, and Ti-VAMP/VAMP7, which we also find on FM4-64-labeled astroglial organelles.

Another difference from neuronal exocytosis is the double requirement for extracellular $Ca^{2+}$ and internal store-operated $Ca^{2+}$. When pharmacologically abolishing with thapsigargin the $Ca^{2+}$ component from intracellular stores, the remaining spatially confined small-amplitude $Ca^{2+}$ signal evoked by m-Stim fails to trigger exocytosis. The indirect mechanical mobilization of $Ca^{2+}$ from thapsigargin-sensitive stores results in a uniform intracellular $Ca^{2+}$ signal, indicating that most $Ca^{2+}$ triggering lysosomal exocytosis is store-operated. Future studies must identify the involvement of the different reticular, vesicular, and mitochondrial $Ca^{2+}$ stores.

**Astroglial lysosomes do not kiss and run**

Our experiments designed to probe the size of the readily releasable pool of lysosomes estimate that astroglial exocytosis mobi-

lizes at most a subset of 20–25% of lysosomes. If we relate the secretory response to m-Stim to this pool size, we can calculate a release probability of ~0.2 for astroglial secretory lysosomes. At the single-lysosome level, exocytosis involves the rapid and total release of FM dye followed by the slower and complete loss of EGFP-sialin, indicating that the lysosome membrane fully collapses into the plasma membrane. These results discard the possibility that the low number of fusion events is compensated for by successive rounds of partial release and rapid refilling of the same organelle (Chen et al., 2005; Bowser and Khakh, 2007; Zhang et al., 2007). The apparent partial release of FM dye observed previously can be explained by a change in FM background signal on stimulation, possibly because of the opening of TRP-like channels (Golovina, 2005) and efflux of dye through FM1-43 permeable pores (Gale et al., 2001). Further studies are needed to elucidate the details of this pathway, which, at the same time, could offer a mechanistic explanation for our observation of an unusual FM uptake into astrocytes.

### Conclusion

Although we do not exclude rapid release of gliotransmitters from astroglia by mechanisms other than exocytosis (Evanko et al., 2004; Takano et al., 2005), our study provides no argument in favor of a contribution of a fast $Ca^{2+}$-regulated exocytic release to this process. Activated at physiological cytosolic $Ca^{2+}$ concentrations, the observed $Ca^{2+}$-dependent release of a subset of astrocytic secretory lysosomes operates on a timescale orders of magnitude slower than neurotransmission. Although our results cannot be directly extrapolated to the situation in tissue, they clearly raise the question of the functional importance of the lysosomal exocytosis in the brain. We show that pathological membrane rupture or massive $[Ca^{2+}]$ elevations after membrane permeabilization with a $Ca^{2+}$ ionophore are more effective in triggering lysosomal exocytosis than physiological $Ca^{2+}$ elevations. Lysosomes have been considered to be a major storage site of immune-signaling substances, such as proinflammatory cytokines (Andrei et al., 2004) and adenosine (Pisoni and Thoene, 1989; Lukashev et al., 2004), and has been implicated in intercellular communication at the immunological synapse (McNeil and Kirchhausen, 2005). Therefore, astrocytic lysosomal exocytosis might be an intrinsic protective response to pathological insults, providing a general mechanism to modulate inflammatory processes in the brain.

## References


Advani RJ, Yang B, Prekeris R, Lee KC, Klumperman J, Scheller RH (1999) VAMP-7 mediates vesicular transport from endosomes to lysosomes. J Cell Biol 146:765–776.

Andrei C, Margiocco P, Poggi A, Lotti LV, Torrisi MR, Rubartelli A (2004) Phospholipases C and A2 control lysosome-mediated IL-1 beta secretion: implications for inflammatory processes. Proc Natl Acad Sci U S A 101:9745–9750.

Andrews NW (2000) Regulated secretion of conventional lysosomes. Trends Cell Biol 10:316–321.

Araque A, Sanzgiri RP, Parpura V, Haydon PG (1998) Calcium elevation in astrocytes causes an NMDA receptor-dependent increase in the frequency of miniature synaptic currents in cultured hippocampal neurons. J Neurosci 18:6822–6829.

Bergles DE, Diamond JS, Jahr CE (1999) Clearance of gluatamate inside the synapse and beyond. Curr Opin Neurobiol 9:293–298.

Betz WJ, Mao F, Bewick GS (1992) Activity-dependent fluorescent staining and destaining of living vertebrate motor nerve terminals. J Neurosci 12:363–375.

Bezzi P, Carmignoto G, Pasti L, Vesce S, Rossi D, Rizzini BL, Pozzan T, Volterra A (1998) Prostaglandins stimulate calcium-dependent glutamate release in astrocytes. Nature 391:281–285.

Bezzi P, Gundersen V, Galbete JL, Seifert G, Steinhäuser C, Pilati E, Volterra A (2004) Astrocytes contain a vesicular compartment that is competent for regulated exocytosis of glutamate. Nat Neurosci 7:613–620.

Bowser DN, Khakh BS (2007) Two forms of single-vesicle astrocyte exocytosis imaged with total internal reflection microscopy. Proc Natl Acad Sci U S A 104:4212–4217.

Chavez RA, Miller SG, Moore HP (1996) A biosynthetic regulated secretory pathway in secretory cells. J Cell Biol 133:1177–1791.

Chen X, Wang L, Zhou Y, Zheng LH, Zhou Z (2005) "Kiss-and-run" glutamate secretion in cultured and freshly isolated rat hippocampal astrocytes. J Neurosci 25:9236–9243.

Chilcote TJ, Galli T, Mundigl O, Edelmann L, McPherson PS, Takei K, De Camilli P (1995) Cellubrevin and synaptobrevins: similar subcellular localization and biochemical properties in PC12 cells. J Cell Biol 129:219–231.

Coco S, Calegari F, Pravettoni E, Pozzi D, Taverna E, Rosa P, Matteoli M, Verderio C (2003) Storage and release of ATP from astrocytes in culture. J Biol Chem 278:1354–1362.

Coorssen JR, Schmitt H, Almers W (1996) $Ca^{2+}$ triggers massive exocytosis in Chinese hamster ovary cells. EMBO J 15:3787–3791.

Crippa D, Schenk U, Francolini M, Rosa P, Verderio C, Zonta M, Pozzan T, Matteoli M, Carmignoto G (2006) Synaptobrevin2-expressing vesicles in rat astrocytes: insights into molecular characterization, dynamics and exocytosis. J Physiol 570:567–582.

Evanko DS, Zhang Q, Zorec R, Haydon PG (2004) Defining pathways of loss and secretion of chemical messengers from astrocytes. Glia 47:233–240.

Fellin T, Carmignoto G (2004) Neurone-to-astrocyte signalling in the brain represents a distinct multifunctional unit. J Physiol 559:3–15.

Fiacco TA, Agulhon C, Taves SR, Petravicz J, Casper KB, Dong X, Chen J, McCarthy KD (2007) Selective stimulation of astrocyte calcium in situ does not affect neuronal excitatory synaptic activity. Neuron 54:611–626.

Gale JE, Marcotti W, Kennedy HJ, Kros CJ, Richardson GP (2001) FM1-43 dye behaves as a permeant blocker of the hair-cell mechanotransducer channel. J Neurosci 21:7013–7025.

Golovina VA (2005) Visualization of localized store-operated calcium entry in mouse astrocytes. Close proximity to the endoplasmic reticulum. J Physiol 564:737–749.

Gordon GR, Mulligan SJ, MacVicar BA (2007) Astrocyte control of the cerebrovasculature. Glia 55:1214–1221.

Harata NC, Choi S, Pyle JL, Aravanis AM, Tsien RW (2006) Frequency-dependent kinetics and prevalence of kiss-and-run and reuse at hippocampal synapses studied with novel quenching methods. Neuron 49:243–256.

Haydon PG, Carmignoto G (2006) Astrocyte control of synaptic transmission and neurovascular coupling. Physiol Rev 86:1009–1031.

Hertz L, Peng L, Dienel GA (2007) Energy metabolism in astrocytes: high rate of oxidative metabolism and spatiotemporal dependence on glycolysis/glycogenolysis. J Cereb Blood Flow Metab 27:219–249.

Hua X, Malarkey EB, Sunjara V, Rosenwald SE, Li WH, Parpura V (2004) $Ca^{2+}$-dependent glutamate release involves two classes of endoplasmic reticulum $Ca^{2+}$ stores in astrocytes. J Neurosci Res 76:86–97.

Jaiswal JK, Chakrabarti S, Andrews NW, Simon SM (2004) Synaptotagmin VII restricts fusion pore expansion during lysosomal exocytosis. PLoS Biol 2:1224–1232.

Jaiswal JK, Fix M, Takano T, Nedergaard M, Simon SM (2007) Resolving vesicle fusion from lysis to monitor calcium-triggered lysosomal exocytosis in astrocytes. Proc Natl Acad Sci U S A 104:14151–14156.

Jourdain P, Bergersen LH, Bhaukaurally K, Bezzi P, Santello M, Domercq M, Matute C, Tonello F, Gundersen V, Volterra A (2007) Glutamate exocytosis from astrocytes controls synaptic strength. Nat Neurosci 10:331–339.

Kreft M, Stenovec M, Rupnik M, Grilc S, Krzan M, Potokar M, Pangrsic T, Haydon PG, Zorec R (2004) Properties of $Ca^{2+}$-dependent exocytosis in cultured astrocytes. Glia 46:437–445.

Krzan M, Stenovec M, Kreft M, Pangrsic T, Grilc S, Haydon PG, Zorec R (2003) Calcium-dependent exocytosis of atrial natriuretic peptide from astrocytes. J Neurosci 23:1580–1583.

Lukashev D, Ohta A, Apasov S, Chen JF, Sitkovsky M (2004) Cutting edge: physiologic attenuation of proinflammatory transcription by the Gs protein-coupled A2A adenosine receptor in vivo. J Immunol 173:21–24.

Luzio JP, Pryor PR, Bright NA (2007) Lysosomes: fusion and function. Nat Rev Mol Cell Biol 8:622–632.

Martinez-Arca S, Alberts P, Zahraoui A, Louvard D, Galli T (2000) Role of tetanus neurotoxin insensitive vesicle-associated membrane protein (TI-VAMP) in vesicular transport mediating neurite outgrowth. J Cell Biol 149:889–900.

McNeil PL, Kirchhausen T (2005) An emergency response team for membrane repair. Nat Rev Mol Cell Biol 6:499–505.

Metzelaar MJ, Wijngaard PL, Peters PJ, Sixma JJ, Nieuwenhuis HK, Clevers HC (1991) CD63 antigen. A novel lysosomal membrane glycoprotein, cloned by a screening procedure from intracellular antigens in eucaryotic cells. J Biol Chem 266:3239–3245.

Meyers JR, MacDonald RB, Duggan A, Lenzi D, Standaert DG, Corwin JT, Corey DP (2003) Lighting up the senses: FM1-43 loading of sensory cells through nonselective ion channels. J Neurosci 23:4054–4065.

Montana V, Malarkey EB, Verderio C, Matteoli M, Parpura V (2006) Vesicular transmitter release from astrocytes. Glia 54:700–715.

Morin P, Sagné C, Gasnier B (2004) Functional characterization of wild-type and mutant human sialin. EMBO J 23:4560–4570.

Mothet JP, Pollegioni L, Ouanounou G, Martineau M, Fossier P, Baux G (2005) Glutamate receptor activation triggers a calcium-dependent and SNARE protein-dependent release of the gliotransmitter D-serine. Proc Natl Acad Sci U S A 102:5606–5611.

Nadrigny F, Rivals I, Hirrlinger PG, Koulakoff A, Personnaz L, Vernet M, Allioux M, Chaumeil M, Ropert N, Giaume C, Kirchhoff F, Oheim M (2006) Detecting fluorescent protein expression and co-localisation on single secretory vesicles with linear spectral unmixing. Eur Biophys J 35:533–547.

Nadrigny F, Li D, Kemnitz K, Ropert N, Koulakoff A, Rudolph S, Vitali M, Giaume C, Kirchhoff F, Oheim M (2007) Systematic co-localization errors between acridine orange and EGFP in astrocyte vesicular organelles. Biophys J 93:969–980.

Nedergaard M, Takano T, Hansen AJ (2002) Beyond the role of glutamate as a neurotransmitter. Nat Rev Neurosci 3:748–755.

Nett WJ, Oloff SH, McCarthy KD (2002) Hippocampal astrocytes *in situ* exhibit calcium oscillations that occur independent of neuronal acitivity. J Neurophysiol 87:528–537.

Ninomiya Y, Kishimoto T, Miyashita Y, Kasai H (1996) $Ca^{2+}$-dependent exocytotic pathways in Chinese hamster ovary fibroblasts revealed by a caged-$Ca^{2+}$ compound. J Biol Chem 271:17751–17754.

Nishikawa S, Sasaki F (1996) Internalization of styryl dye FM1-43 in the hair cells of lateral line organs in *Xenopus* larvae. J Histochem Cytochem 44:733–741.

Pangrsic T, Potokar M, Stenovec M, Kreft M, Fabbretti E, Nistri A, Pryazhnikov E, Khiroug L, Giniatullin R, Zorec R (2007) Exocytotic release of ATP from cultured astrocytes. J Biol Chem 282:28749–28758.

Parpura V, Fang Y, Basarsky T, Jahn R, Haydon PG (1995) Expression of synaptobrevin II, cellubrevin and syntaxin but not SNAP-25 in cultured astrocytes. FEBS Lett 377:489–492.

Parri HR, Crunelli V (2003) The role of $Ca^{2+}$ in the generation of spontaneous astrocytic $Ca^{2+}$ oscillations. Neuroscience 120:979–992.

Perea G, Araque A (2007) Astrocytes potentiate transmitter release at single hippocampal synapses. Science 317:1083–1086.

Pisoni RL, Thoene JG (1989) Detection and characterization of a nucleoside transport system in human fibroblast lysosomes. J Biol Chem 264:4850–4856.

Pryazhnikov E, Khiroug L (2008) Sub-micromolar increase in $[Ca^{2+}]_i$ triggers delayed exocytosis of ATP in cultured astrocytes. Glia 56:38–49.

Rao SK, Huynh C, Proux-Gillardeaux V, Galli T, Andrews NW (2004) Identification of SNAREs involved in synaptotagmin VII-regulated lysosomal exocytosis. J Biol Chem 279:20471–20479.

Rouze NC, Schwartz EA (1998) Continuous and transient vesicle cycling at a ribbon synapse. J Neurosci 18:8614–8624.

Seal RP, Edwards RH (2006) The diverse roles of vesicular glutamate transporter 3. Handb Exp Pharmacol 17:137–150.

Simard M, Nedergaard M (2004) The neurobiology of glia in the context of water and ion homeostasis. Neuroscience 129:877–896.

Stenovec M, Kreft M, Grilc S, Potokar M, Kreft ME, Pangrsic T, Zorec R (2007) $Ca^{2+}$-dependent mobility of vesicles capturing anti-VGLUT1 antibodies. Exp Cell Res 313:3809–3818.

Striedinger K, Meda P, Scemes E (2007) Exocytosis of ATP from astrocyte progenitors modulates spontaneous $Ca^{2+}$ oscillations and cell migration. Glia 55:652–662.

Takano T, Kang J, Jaiswal JK, Simon SM, Lin JH, Yu Y, Li Y, Yang J, Dienel G, Zielke HR, Nedergaard M (2005) Receptor-mediated glutamate release from volume sensitive channels in astrocytes. Proc Natl Acad Sci U S A 102:16466–16471.

Teter K, Chandy G, Quiñones B, Pereyra K, Machen T, Moore HP (1998) Cellubrevin-targeted fluorescence uncovers heterogeneity in the recycling endosomes. J Biol Chem 273:19625–19633.

Volterra A, Meldolesi J (2005) Astrocytes, from brain glue to communication elements: the revolution continues. Nat Rev Neurosci 6:626–640.

Wojcik SM, Rhee JS, Herzog E, Sigler A, Jahn R, Takamori S, Brose N, Rosenmund C (2004) An essential role for vesicular glutamate transporter 1 (VGLUT1) in postnatal development and control of quantal size. Proc Natl Acad Sci U S A 101:7158–7163.

Zhang Q, Pangrsic T, Kreft M, Krzan M, Li N, Sul JY, Halassa M, Van Bockstaele E, Zorec R, Haydon PG (2004a) Fusion-related release of glutamate from astrocytes. J Biol Chem 279:12724–12733.

Zhang Q, Fukuda M, Van Bockstaele E, Pascual O, Haydon PG (2004b) Synaptotagmin IV regulates glial glutamate release. Proc Natl Acad Sci U S A 101:9441–9446.

Zhang Z, Chen G, Zhou W, Song A, Xu T, Luo Q, Wang W, Gu XS, Duan S (2007) Regulated ATP release from astrocytes through lysosome exocytosis. Nat Cell Biol 9:945–953.